Petroleum Science 21 (2024) 4153–4164

Contents lists available at ScienceDirect

Petroleum Science

journal homepage: www.keaipublishing.com/en/journals/petroleum-science

Original Paper

Potential application of wet-phase modified expandable graphite particles as a novel in-depth profile control agent in carbonate reservoirs

Bo-Zhao Xu [a, b], Dong-Fang Lv [a, b], Dai-Yu Zhou [c], Ning Sun [d], Si-Yu Lu [a, b], Cai-Li Dai [a, b], Guang Zhao [a, b, *], Ming-Ming Shi [e]

[a] School of Petroleum Engineering, China University of Petroleum (East China), Qingdao, 266580, Shandong, PR China
[b] State Key Laboratory of Deep Oil and Gas, China University of Petroleum(East China), 266580, Shandong, PR China
[c] CNPC Tarim Oilfield, Korla, 841001, Xinjiang, PR China
[d] SINOPEC Petroleum Exploration and Production Research Institute, Beijing, 102206, PR China
[e] Xianhe Oil Production Plant, SINOPEC Shengli Oilfield, Dongying, 257068, Shandong, PR China

ARTICLE INFO

Article history:
Received 23 January 2024
Received in revised form
13 June 2024
Accepted 4 July 2024
Available online 6 July 2024

Edited by Yan-Hua Sun

Keywords:
WMEG particles
In-depth profile control
Resistance of temperature and salinity
EOR capacity
Fractured carbonate reservoirs

ABSTRACT

Novel wet-phase modified expandable graphite (WMEG) particles were developed for in-depth profile control in carbonate reservoirs. The harsh environment of carbonate reservoirs ($\geq$ 130 °C, $\geq$ 22 $\times$ 10^4 mg/L) brings significant challenges for existing profile control agents. WMEG particles were developed to address this problem. WMEG particles were synthesized via intercalation with ultrasound irradiation and chemical oxidation. The critical expansion temperature of WMEG particles is 130 °C, and these particles can effectively expand 3–8 times under high temperature and high salinity water. The core flow experiments show that WMEG particles exhibit a good plugging capacity, profile control capacity, and a better-enhanced oil recovery (EOR) capacity in deep carbonate reservoirs. WMEG particles can be expanded in the formation and form larger particles that bridge the upper and lower end faces of the fracture. Then the high-permeability zones are effectively plugged, and the heterogeneity is improved, resulting in an obvious increase in oil recovery. This research provides a novel insight into future applications of profile control agents for in-depth profile control treatment in carbonate reservoirs.

1. Introduction

About 40% of the global oil and gas reserves are located in carbonate reservoirs, while these reservoirs account for 60% of the world's production (Dai et al., 2018; Liu et al., 2022). With a wide distribution worldwide, carbonate reservoirs play a significant role in the production of oil and gas on a global scale (Alshehri et al., 2019; Wu et al., 2015). Carbonate reservoirs are mainly fractured reservoirs whose permeability is hundreds of times higher than that of matrix permeability and are extremely heterogeneous. During the water flooding process, the injected fluid inclines to flow through fractures and ultimately reaches the production well (Lu et al., 2022). This results in a rapid increase in water cut and limits the recovery of carbonate fractured reservoirs to approximately 35%, seriously constraining the efficient exploitation (Asl et al., 2022). The efficient exploitation of carbonate fractured reservoirs faces a significant challenge is that how to develop a temperature and salt resistance profile control technology that reduces the water cut. In summary, the development of effective profile control technologies to reduce the water cut and enhance the recovery of carbonate fractured reservoirs is a vital research direction.

Among them, gel stands out as the most widely used chemical profile control agent in oilfields, which is composed of polymers and crosslinkers (Bruno et al., 2022; Ge et al., 2021; Gussenov et al., 2019; Jin et al., 2021; Mehrabianfar et al., 2020). In recent years, polymer gel and polymer particles with strengthening agents have been applied to carbonate fractured reservoirs (Bai et al., 2022; Wu et al., 2023; Zhu et al., 2022). Taking polymer gel as an example, the temperature and salinity resistance (140 °C, > 24 $\times$ 10^4 mg/L) of

* Corresponding author. School of Petroleum Engineering, China University of Petroleum (East China), Qingdao, 266580, Shandong, PR China.
E-mail address: zhaoguang@upc.edu.cn (G. Zhao).

https://doi.org/10.1016/j.petsci.2024.07.008

polyacrylamide gel was strengthened by adding scleroglucan (USP) and CCH ($CoCl_2 \cdot 6H_2O$) (Wu et al., 2022). However, the gelling performance of gel is not ideal in high temperature and high salt environment, and the degradation speed is accelerated. Foam is composed of a foaming agent and foam stabilizer. In such a harsh environment, it is challenging to preserve the prolonged stability of conventional foam (Boeije and Rossen, 2017). Therefore, some scholars have enhanced the temperature and salinity resistance of foam by adding strengthening agents, such as DPG and nano-graphite. However, its construction cost is too high to be applied to oilfields. Improving the stability of foam agents in harsh environment is one of the most critical problems (Song et al., 2023; Sun et al., 2023). The particle profile control agent exhibits size management properties and can be easily injected into the formation, while the organic particle agent is easily degraded, resulting in an unsatisfactory plugging effect. Inorganic particle agents have good chemical stability, thermal stability and mechanical strength, and are suitable for profile control in harsh reservoir environments. It mustn't be affected by the reservoir environment. Inorganic particle agents mainly include ultrafine cement and silica nanoparticles (Liu et al., 2020; Salem Ragab and Hannora, 2015; Wang et al., 2022). Ultrafine cement has emerged as a novel particle agent for reservoir water plugging in recent years. Characterized by small particle sizes, it easily enters in-depth reservoirs, achieving a high success rate in water plugging applications (Liu et al., 2017). However, there are problems such as fast hydration reactions and short solidification times, so ultrafine cement is generally mixed with inorganic materials to increase the safety of ultrafine cement applications (Gong et al., 2016). Silica nanoparticles are small (1–100 nm), have good dispersion and stability, and can easily penetrate formation pores, so they have been used as drilling fluid and oil displacement agent in oilfield (Almohsin et al., 2021; Luo et al., 2021; Li Q. et al., 2022). The mixture of silica nanoparticles and activator can change the liquid into rigid material in the target layer, efficiently plug the water channels and improve the sweep coefficient of subsequent water flooding. However, the price of silica nanoparticles is too expensive to be applied to oil fields on a large scale (Karadkar et al., 2023). Organic agents have the advantages of low cost and easy injection, but the water plugging effect is unstable and easily affected by environmental factors (Du et al., 2023). Therefore, based on inorganic particles with good chemical stability, a profile control agent suitable for carbonate reservoirs is developed.

Expandable graphite (EG) is a graphite intercalation formed by the chemical treatment of natural flake graphite, such as acid, alkali metal, salt, and other chemical substances, which is widely used in aerospace, automobile, building, fire-retardant, and other fields. As a functional carbon material, EG has the advantages of low density, high strength, size control, thermostability, corrosion resistance, etc. However, the temperature needed for EG expansion is too high (> 400 °C), leading to the formation of worm-like structures in the expanded graphite. This indicates significant damage to the original lamellar structure of graphite, resulting in a loss of its structural strength. The temperature range of the carbonate fractured reservoir is usually 130–200 °C and existing EG will not have good expansion performance under this condition. Additionally, the reservoir environment is a water-phase environment, which significantly weakens the expansion ability of expandable graphite. Therefore, traditional EG particles cannot be used in reservoirs under such conditions. To solve these problems, Zhao and his co-workers (Xu et al., 2023; Zhao et al., 2019) prepared novel expandable graphite particles by optimizing the synthesis steps. As a steam channel profile control agent, the EG particle can expand to a certain extent at steam temperature (300 °C) and control the steam channels for an extended period (Xu et al., 2023; Zhao et al., 2019). The EG particle system has found successful application in the heavy oil block of the Shengli Oilfield in China and has achieved a good oil increase effect (Xu et al., 2023).

Aiming at the carbonate fractured reservoir, a kind of novel wet-phase modified expandable graphite (WMEG) particles is developed by optimizing the synthesis method. The initial expansion temperature of the WMEG particles is 130 °C, and the expansion ratio is 3–8 times higher at 200 °C (in the wet phase). Flow testing in fractured cores are carried out, and the plugging performance and profile control capacity of the WMEG particles were studied. The distribution of WMEG particles in the porous media is analyzed using a scanning electron microscope (SEM) and low-field nuclear magnetic resonance (LF-NMR), and the profile control mechanism is clarified. The mechanism of plugging water channels with the WMEG particles is explored. This study broadens the applications for expandable graphite and provides a new measure for profile control and water plugging in carbonate fractured reservoirs.

2. Materials and methods

2.1. Experimental materials

Natural flake graphite (NFG) particles (50 mesh, carbon content of 99.5%) were purchased from Hengrunda Co. Ltd. of China. $KMnO_4$ (AG, 99.5%), HNO_3 (analytical grade, 68%), $HClO_4$ (analytical grade, 72%), CH_3COOH (AG, 99.5%), H_2C_2O4 (AG, 99%) and $K_2S_2O_8$ (AG, 99%) were purchased from Aladdin Industrial Co. Ltd. of China. SD-2 polymer was synthesized in the laboratory. Simulated water with a salinity of 300,000 mg/L was prepared from NaCl at 280,000 mg/L, $CaCl_2$ at 10,000 mg/L and $MgCl_2$ at 10,000 mg/L. The simulated oil was provided by the Tahe Oilfield of China, and its viscosity was 378 mPa s at 50 °C.

2.2. Preparation of the WMEG particle system

Four steps, including ultrasonic co-oxidation, inorganic acid intercalation, organic acid intercalation, and dry mixing with expansive agents, were used to synthesize the WMEG particle system. The expansive agents include $K_2S_2O_8$ and $H_2C_2O_4$. Among them, the oxidation stage was completed in the ultrasonic cleaning bath, the intercalation stage was performed in the water bath, and all steps were finished at 30 °C. The preparation processes are set as follows. (1) Ultrasonic co-oxidation stage: 2 g of $KMnO_4$ and 20 g of HNO_3 were fully mixed in a beaker. Then, 10 g of NFG particles were added to the mixed solution, and the beaker was placed into an ultrasonic cleaning bath for 60 min (2) Inorganic acid intercalation stage: 40 g of $HClO_4$ was added to the beaker, and the mixture was dispersed for 30 min in a constant-temperature water bath. (3) Organic acid intercalation stage: 30 g of CH_3COOH was then added to the mixture, and the sealed beaker was still in a water bath at 30 °C for 30 min. After the completed reaction, the obtained particles were washed with ultrapure water until they reached a neutral state and then dried for 12 h at 60 °C. (4) Dry mixing with expansive agent: 1 g $K_2S_2O_8$, 1 g $H_2C_2O_4$ and 2 g SD-2 polymer were poured into the product, and mixed well to obtain the WMEG particle system. Fig. 1 illustrates the synthetic route of the WMEG particle system.

2.3. Characterization of the WMEG particles

The structure of the WMEG particles was characterized by a Nicolet 6700 Fourier transform infrared spectrometer (Thermo Scientific, USA). The X-ray diffraction of WMEG particles was analyzed by a D8 Advance X-ray diffraction instrument (Bruker, Switzerland). The morphology of the WMEG particles was observed

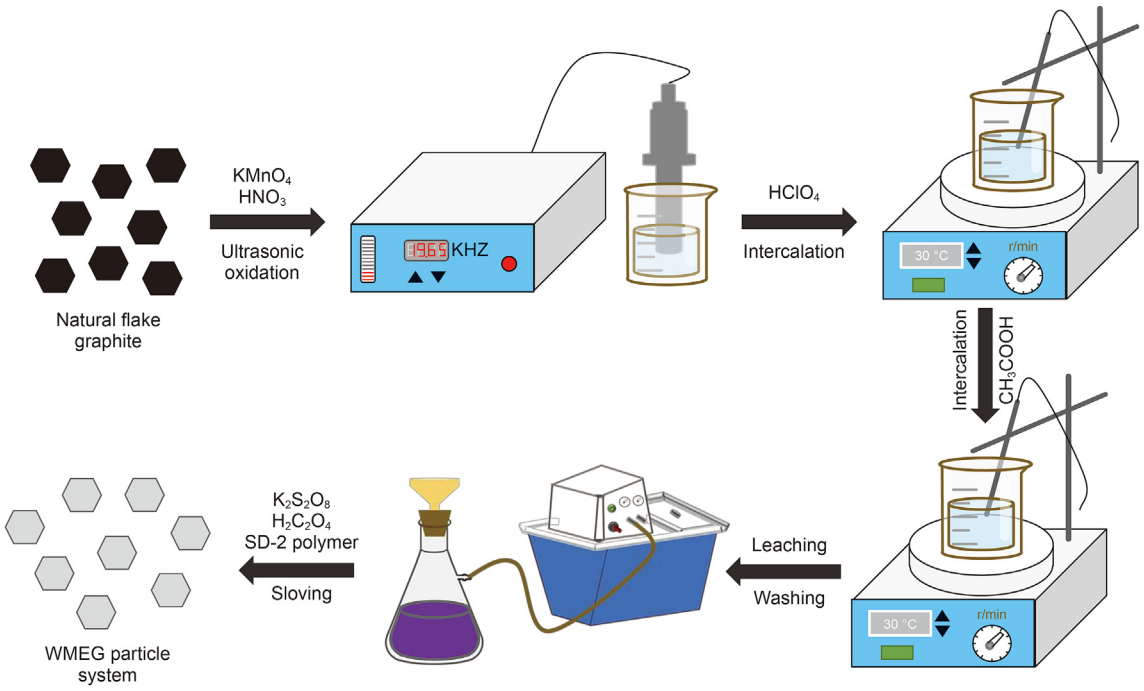

Fig. 1. Synthetic route of the WMEG particle system.

using a Hitachi S-4800 scanning electron microscope (SEM, Hitachi, Japan).

2.4. Expansion performance of the WMEG particles

Different reservoir temperatures and salinities were simulated to investigate the reservoir application of the WMEG particles. 1 g of WMEG particles and 10 g of simulated water were put into a hydrothermal reaction vessel. The expansion capacity of the WMEG particles was recorded at different temperatures, salinities, pressures, and aging times.

2.5. Plugging experiments of the WMEG particles

The plugging capacity of WMEG particles were evaluated using a single core flow experiment. The core flow chart is shown in Fig. 2.

When conducting these plugging capacity experiments, five cores with different fracture sizes were injected with 3 fracture volumes (FVs) of the 1% WMEG particles, and then aged at 200 °C for 2 d. Sequentially, several FVs of simulated water were injected into cores until the injection pressure stabilized. The injection pressure was recorded during the procedure to determine the resistance factor and plugging rate. To describe the matching relationship between the median particle size of the WMEG particles and fracture, the matching coefficient f is introduced. The matching coefficient is defined as the ratio of the median diameter of particles to the equivalent width of the fracture (Ding et al., 2021):

$$f = \frac{D_{50}}{w} \tag{1}$$

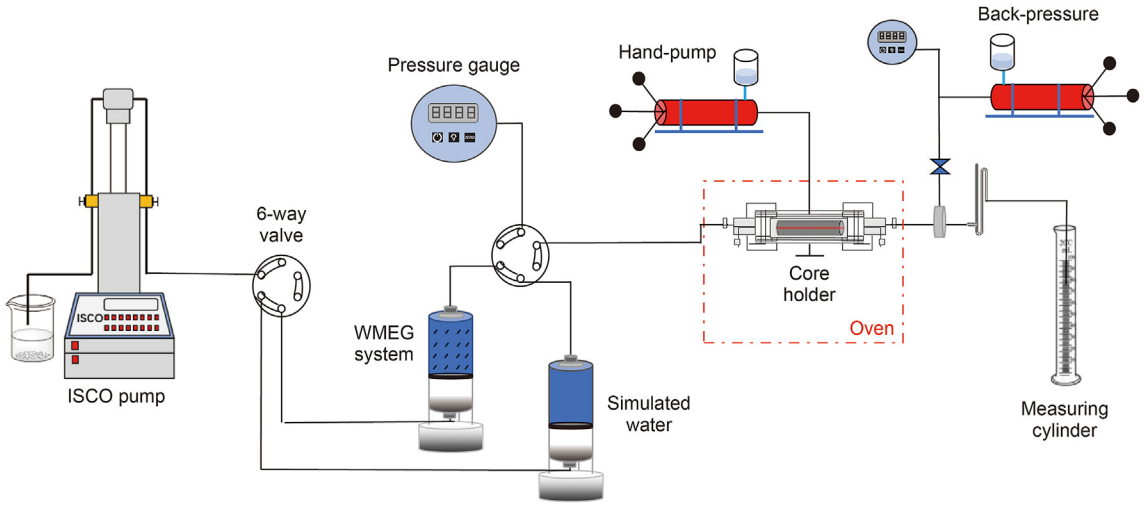

Fig. 2. The chart of flow testing in single cores.

$$R_p = \frac{k_b - k_a}{k_b} \quad (2)$$

where f is the matching coefficient; D_{50} is the median diameter of the system, μm; and w is the fracture width, μm; R_p the plugging rate; k_a is the permeability of the core after injection and expansion of WMEG particles, μm^2; and k_b is the permeability of the core before injection of WMEG particles, μm^2.

2.6. In-depth profile control experiments of the WMEG particles

Flow testing in parallel cores were used in this section. The flow chart of parallel cores is shown in Fig. 3. To simulate the heterogeneity of the formation, four groups of parallel cores with varying permeability ratios were utilized. First, simulated water was injected into these parallel cores until the injection pressure and produced water reached a steady state. Second, 3 FVs of a 1% WMEG particle solution were injected into these parallel cores and then aged for 2 d at 200 °C. Third, several PVs of simulated water were injected into these parallel cores until the injection pressure and produced water became stable again. To determine the profile control rate, the produced water output was recorded in this process.

2.7. EOR capacity of the WMEG particles

To measure the NMR T_2 spectra and NMR images, nuclear magnetic resonance was used (Macro MR12-150H–I, Suzhou Niumag Analytical Instrument Co., Ltd., China). Fig. 4 shows the flow chart of the NMR device. (1) The core was successively saturated with simulated water and simulated oil. (2) Simulated water was injected until the water cut of the produced liquid reached 98%. (3) 3 FVs of the 1% WMEG particle solution were injected into the core, and the core was aged in a 200 °C oven for 2 d. (4) Simulated water was injected again until the water cut reached 100%. The injection rate were set to 1% and 1 mL/min, respectively. To remove the signal from hydrogen atoms, heavy water was used as the simulated water.

3. Results and discussion

3.1. FT-IR analysis of WMEG particles

Fig. 5 shows FT-IR spectra of NFG particles, WMEG particles, and expanded WMEG particles. As seen from the spectra of the WMEG particles, the relatively strong characteristic peaks at 1086 and 629 cm^{-1} are ascribed to ClO_4^- and Cl–O, respectively. The characteristic peak at 1383 cm^{-1} is attributed to the presence of NO_3^-. Other peaks in the 1150–1050 cm^{-1} are attributed to the absorption of oxygen-containing groups. The results demonstrate that nitrate groups and perchlorate groups were successfully intercalated into the graphite interlayers. Furthermore, the characteristic peak at 1632 cm^{-1} is contributed by the C=O stretching vibration in –COOH, while the peak at 2926 cm^{-1} is ascribed to antisymmetric stretching and symmetrical stretching of methylene. A wide adsorption zone at approximately 3444 cm^{-1} is due to the –OH groups. The results indicate that oxygen-containing groups were effectively formed due to the oxidizing action of the combination intercalation method.

Compared with WMEG particles, all characteristic peaks of expanded WMEG particles were quite weaker than the former, indicating the thermal decomposition of intercalated compounds after heating WMEG particles for expansion. In addition, the peak at 1632 cm^{-1} detected in these three curves corresponds to the stretching vibration of C–C, which indicates that the carbon hexagonal ring of NFG particles was maintained after oxidization, intercalation, and expansion procedures. The addition of potassium persulfate will not cause the formation of functional groups with oxidation characteristics in graphite.

3.2. X-ray diffraction analysis of WMEG particles

Fig. 6 demonstrates the XRD patterns of the NFG particles, WMEG particles, and expanded WMEG particles. For NFG particles, the two characteristic peaks were at $2\theta = 26.53°$ (002) and $2\theta = 54.67°$ (004), with high intensities and sharp shapes. These features indicate that the arrangement mode of carbon atoms inside the NFG particles was regular and that the material was highly crystallized. After oxidation treatment, the main diffraction peaks of the WMEG particles had decreased intensities and wider ranges. The diffraction peak of the NFG particles at $2\theta = 26.53°$ was

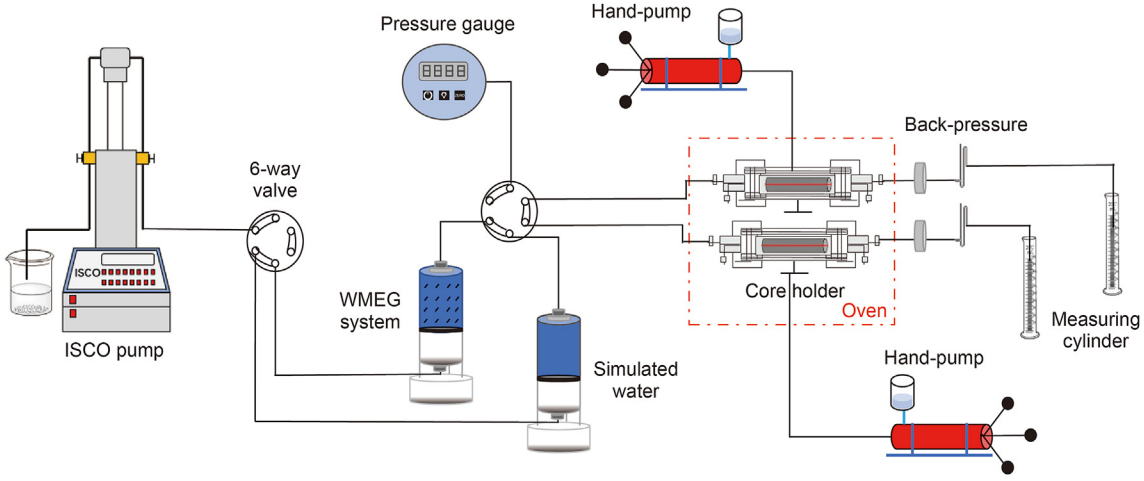

Fig. 3. The chart of flow testing in parallel cores.

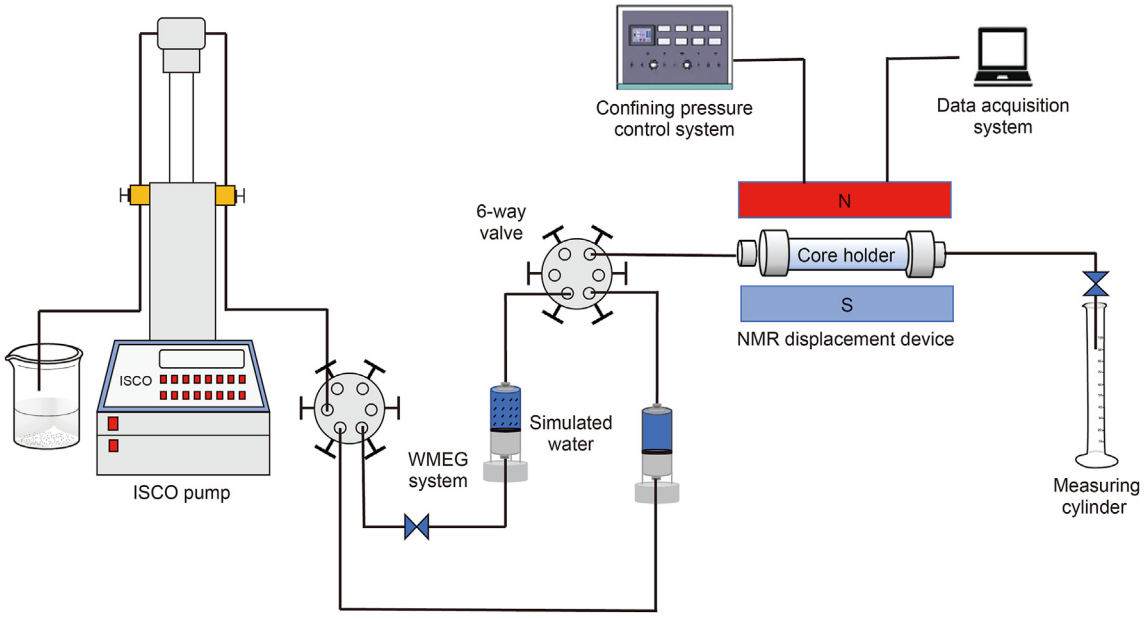

Fig. 4. The flow chart of NMR displacement device.

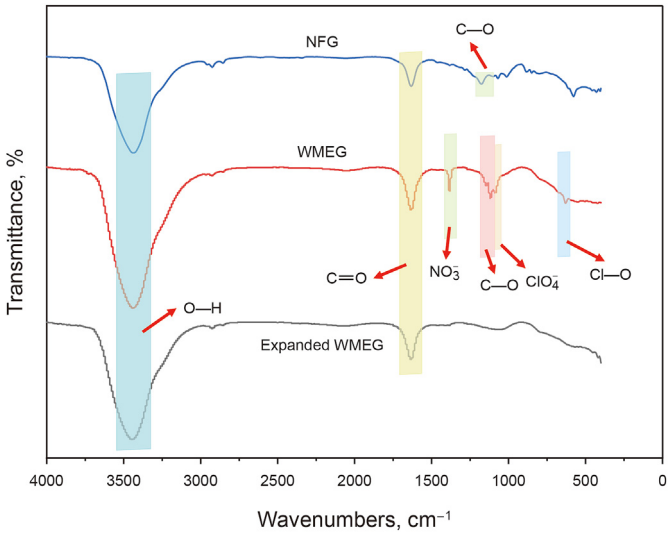

Fig. 5. FT-IR spectra of NFG particles, WMEG particles, and expanded WMEG particles.

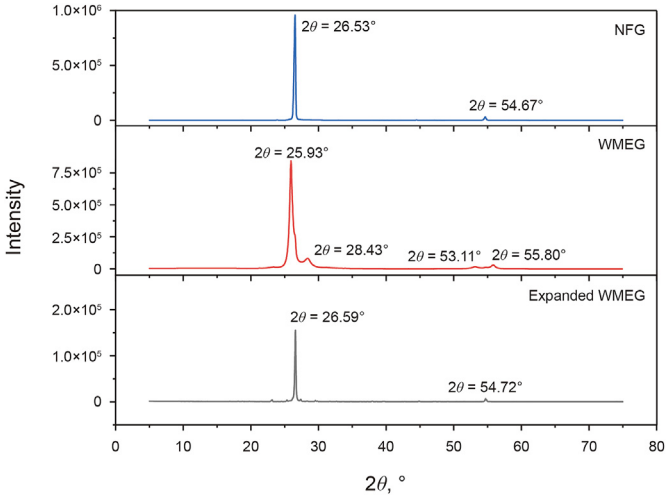

Fig. 6. X-ray diffraction patterns of NFG particles, WMEG particles, and expanded WMEG particles.

separated into two peaks at $2\theta = 25.93°$ and $2\theta = 28.43°$, which indicated that graphite microcrystals were partially oxidized. The diffraction peak was also divided into two independent peaks, resulting from the intercalation process of agents into the layer spacing. Oxygen-containing groups were effectively grafted onto the surface of the graphite layer, which enlarged the interlayer distance and decreased the diffraction angle. The intensities of the characteristic peaks were markedly decreased after thermal expansion which indicated that the diffraction angles of expanded WMEG particles were similar to those of NEG particles. During the heating treatment, the intercalation agents inside the graphite layers decomposed, and the expanded WMEG particles changed into a more porous structure, causing a reduction in the microcrystalline nature of the NEG particles. Therefore, the remaining characteristic peaks indicated that the WMEG particles were successfully synthesized.

3.3. Morphology of NFG particles and WMEG particles

Fig. 7 shows typical morphologies of NFG particles and WMEG particles before aging. NFG is a lamellar structure, which is formed by stacking a large amount of graphite layers (Fig. 7(a)–(c)). The surface of NFG particles are smooth. After the above ultrasonic irradiation and chemical oxidation treatment, a large number of salt particles remain on the surface of the WMEG particles (Fig. 7(d)–(f)). The dense lamellar structure is destroyed and the interlayer spacing becomes wider. The changes in the layer structures result from the destruction of hybrid bonds in the carbon hexagonal plate, contributing to the curling and bulging of the border, and then the intercalation compounds approach the layer of graphite to increase the interlayer spacing.

Fig. 8 shows the microstructure of the NFG particles and WMEG particles after aging. After 2 d of aging, the microstructure of the NFG particles has no obvious change but still maintains the lamellar

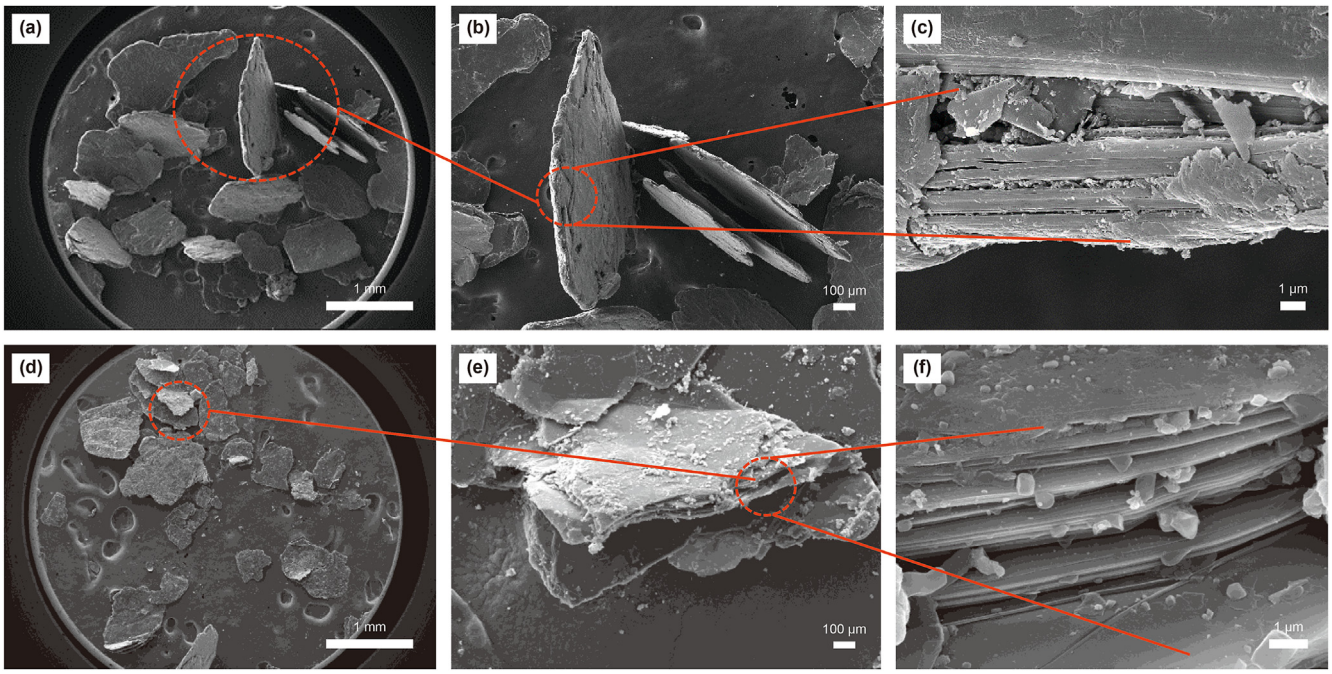

Fig. 7. SEM morphologies of NFG particles and WMEG particles. (**a**)–(**c**) Original morphologies of NFG particles; (**d**)–(**f**) Original morphologies of WMEG particles.

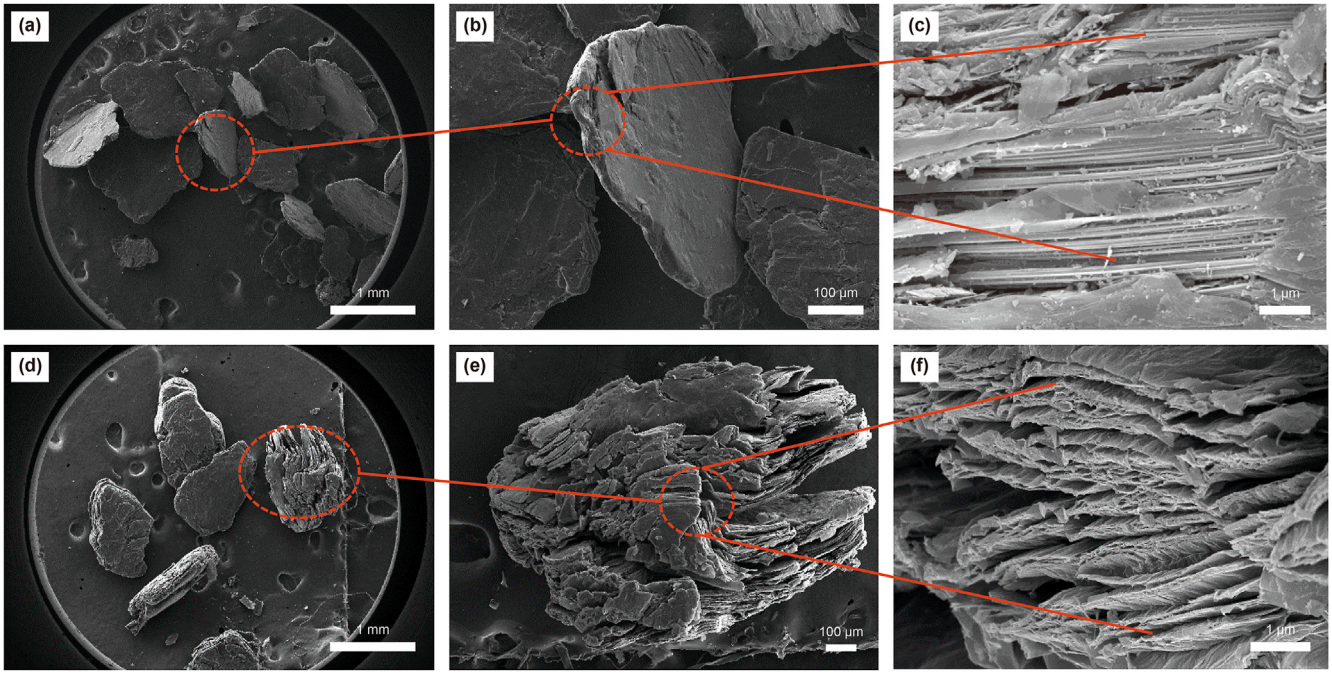

Fig. 8. SEM morphologies of NFG particles and WMEG particles after aging. (**a**)–(**c**) Morphologies of NFG particles after aging; (**d**)–(**f**) Morphologies of WMEG particles after aging.

structure, and the graphite layer is closely connected with the graphite layer (Fig. 8(a)–(c)). After aging, the microstructure of the WMEG particles changes obviously. The graphite layer is opened, and the spacing is enlarged, but the lamellar structure is still maintained. This is because the aging temperature is too low, and the decomposition of the intercalation agent is incomplete. The original structure of WMEG particles has not been destroyed, the expansion ratio is limited, and it does not become a worm-like structure (Fig. 8(d)–(f)). This ensures the structural strength of WMEG particles in the plugging process.

3.4. The effect of temperature and salinity on the expansive performance

In this work, the expansion ratio is defined as the ratio of the expansion volume to the beginning volume to characterize the expansive performance of the WMEG particles. Fig. 9 shows that the expansion ratio is greater at higher temperature. The initial

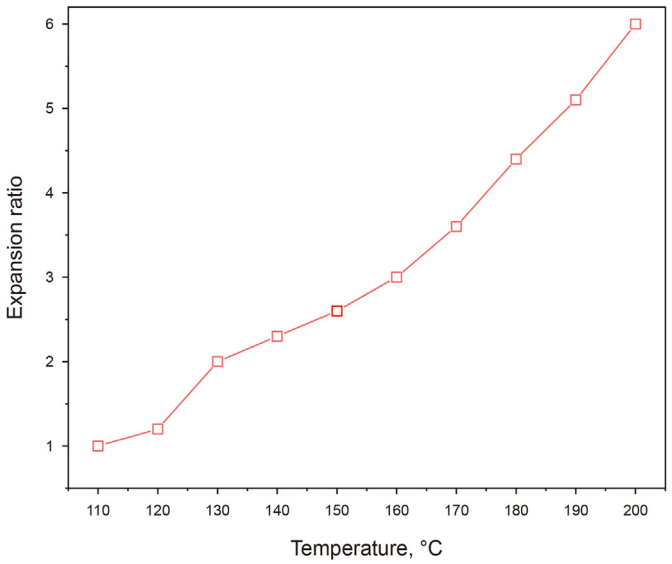

Fig. 9. Expansion ratio of the WMEG particles at different temperatures.

critical expansion temperature of the WMEG particles is 130 °C. The high temperature has an obvious effect on the expansion performance of the WMEG particles. This can be related to the gas release rate of the intercalation agents. Generally, the intercalation agents inside the graphite sheets are easily decomposed to release gases at higher temperatures and then produce a faster release rate of gas. The rapid release rate of gas will produce a greater instantaneous impetus between graphite sheets, thus enlarging the distance between sheets of the WMEG particles. Additionally, the gas of intercalation agents is released more completely at high temperature than at low temperature. Therefore, at high temperatures, the final expansion ratio of the WMEG particle system is greater than that at low temperatures.

The expansion experiments of the WMEG particle system were carried out in low-salinity water and high-salinity water ($0-30 \times 10^4$ mg/L) at 200 °C for 1 d. In this experiment, NaCl, $CaCl_2$, and $MgCl_2$ were used to prepare simulated water. The experimental results are shown in Fig. 10. Within the range of 300,000 mg/L, the expansion performance of the WMEG particles does not change significantly with an increase in formation water salinity. This is because the WMEG particles is an inorganic particle with chemical inertia and will not react with salts. Therefore, salinity does not affect the expansion performance of the WMEG particles.

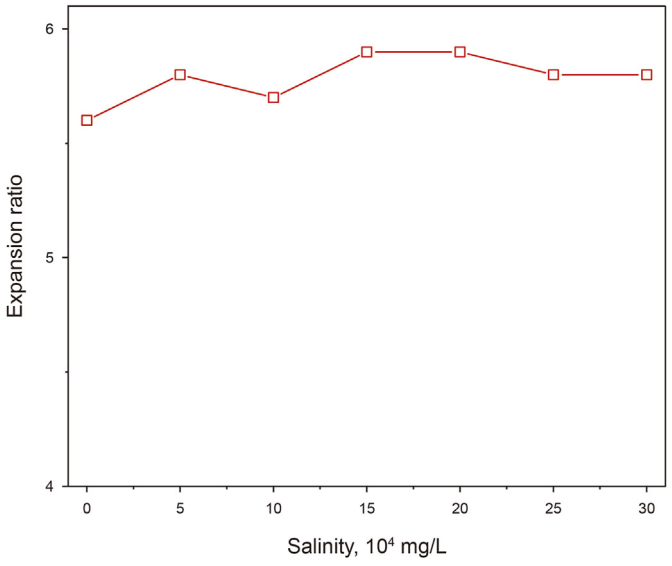

Fig. 10. Expansion ratio of the WMEG particles in different salinity formation water.

3.5. The effect of aging time on the expansion capacity

As the aging time increased, the expansion ratio of the WMEG particles at different temperatures increased rapidly in the initial time (Fig. 11(a)). It is noted that the expansion ratio reached the maximum after aging for 9 d while the expansion ratio almost no longer changed in the following 6 d. This is because the intercalation agents (HNO_3, $HClO_4$) and expansive agent ($K_2S_2O_8$) of the WMEG particles decomposed and released a large amount of gas at the initial stage, resulting in an enlarged distance between the graphite sheets. When continuously aging, the decomposition procedure of the intercalation agents was completed and the gases were no longer produced. This may be related to the van der Waals of graphite and the force generated by the gas of intercalation agents. When the van der Waals is smaller than the force generated by the gas, the sheet will be expanded in a direction vertical to the sheet surface. However, the amount of released gas gradually decreases as the aging time increases which results in insufficient driving forces between graphite sheets. Therefore, the distance between the graphite sheets remains nearly constant over the following aging days. It was also observed that the expansion time of the WMEG particles in high-salinity water increased more slowly than that in low-salinity water. However, both of these the WMEG particles almost reached the same expansion ratio after being fully aged in simulated water with 300,000 mg/L (Fig. 11(b)). This indicates that the presence of salt particles in the system only influences the initial stage of the expansion process, and the WMEG particles can exist stably for a long time in water.

3.6. Plugging capacity of the WMEG particles

First, five kinds of cores with different fracture widths were designed, and the corresponding fracture width-WMEG particle size matching coefficients were calculated according to Eq. (1), as shown in Table 1. Fig. 12(a) shows the injection pressure change for the WMEG particles during injection. The density of the WMEG particles before expansion is greater than that of water and tends to deposit to the bottom, while the previously added SD-2 polymer improves the suspension capacity of the WMEG particles, which makes it easy to enter the deep fracture. The WMEG particles plug the flow channel mainly by direct plugging and expansion plugging. The injected WMEG particles resist the flow of the whole fracture through the bridge fracture. This causes the injection pressure to increase continuously. When the matching coefficient is 0.06, the injection pressure increases slowly, which is lower than the other four groups of experiments. The width of the fracture is too large, so the injected WMEG particles cannot reduce the fluidity of the fracture. Due to the effect of gravity, all WMEG particles accumulate on the lower fracture end-face, and WMEG particles do not form direct plugging in the fracture. When the matching coefficient is 0.1, the injection pressure reaches the maximum. This results from the retention and accumulation of WMEG particles after entering the fracture smoothly. A high matching coefficient results in a decrease in the width of the crack, a reduction in the quantity of WMEG particles that enter the fracture, and limited plugging.

Fig. 12(b) shows the change in water flooding pressure after core aging. Compared with that before aging, the injection pressure of

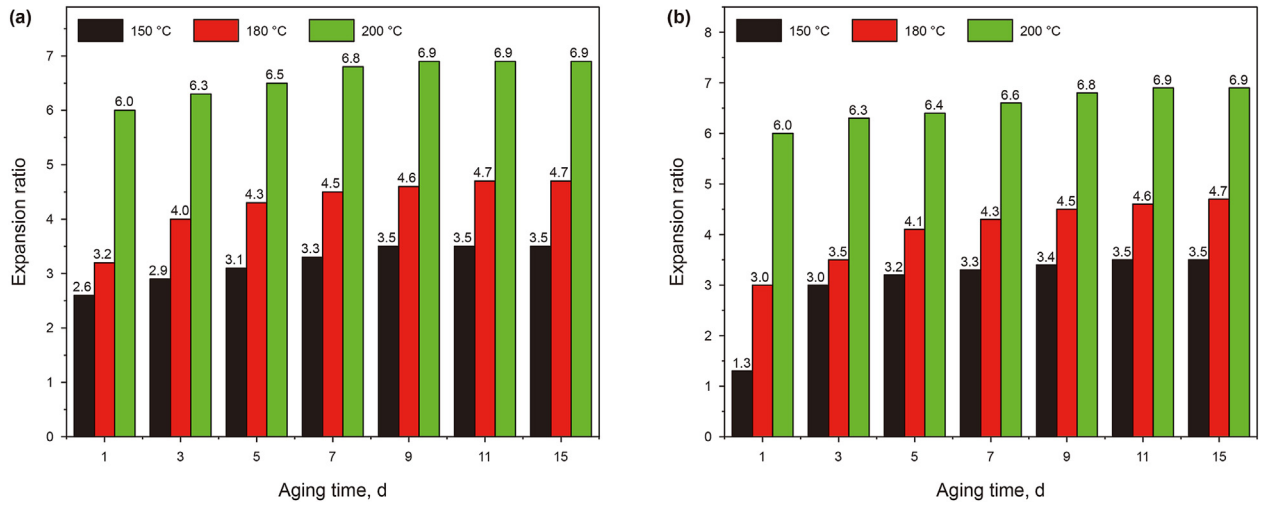

Fig. 11. The WMEG particle expansion ratio in ultra-pure water (**a**) and simulated water with 300,000 mg/L (**b**).

Table 1
Plugging rates under different matching coefficients.

No.	Core parameters			Particle size of WMEG, μm	Matching coefficient	Resistance coefficient	Plugging rate, %
	Diameter, cm	Length, cm	Fracture width, mm				
1	2.502	4.989	1.0	300	0.300	14.95	94.6
2	2.513	4.976	2.0	300	0.150	19.77	96.2
3	2.511	4.998	3.0	300	0.100	22.98	96.9
4	2.505	4.981	4.0	300	0.075	20.39	95.6
5	2.500	4.986	5.0	300	0.060	5.39	88.0

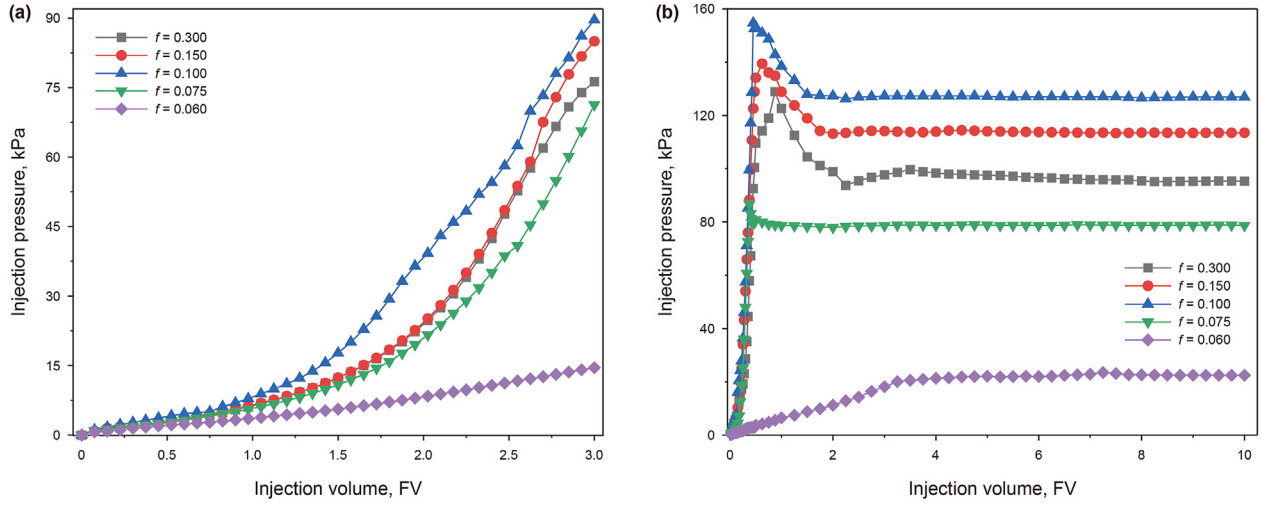

Fig. 12. The injection pressure of the WMEG particles with different matching coefficients. (**a**) Injection of WMEG particles; (**b**) Subsequent water flooding after aging.

the five experiments increases, showing that the expansion effect of the WMEG particles greatly enhances the plugging performance. During the experiment, the injection pressure remains stable under the condition of water flooding for a long time, indicating that the expanded WMEG particles have erosion resistance and can exist stably in the fractured core. However, when the matching coefficient is 0.06, the injection pressure rise is small, which indicates that the expanded WMEG particles are still unable to form effective plugging in large fractures. The injection pressure reaches the maximum when the matching coefficient is 0.1. This is because based on the bridge across the fracture of WMEG particles, the particle size of expanded WMEG particles increases, and the plugging effect is further strengthened. When there is a large matching coefficient, the injection pressure decreases slightly due to the small number of WMEG particles entering the fracture. The plugging effect of expanded WMEG particles is shown in Table 1.

3.7. Profile control capacity of the WMEG particles

Fig. 13 shows the variations in the injection pressure and diversion rate of cores with different fracture width ratios during the whole flooding stage. The core parameters are shown in Table 2.

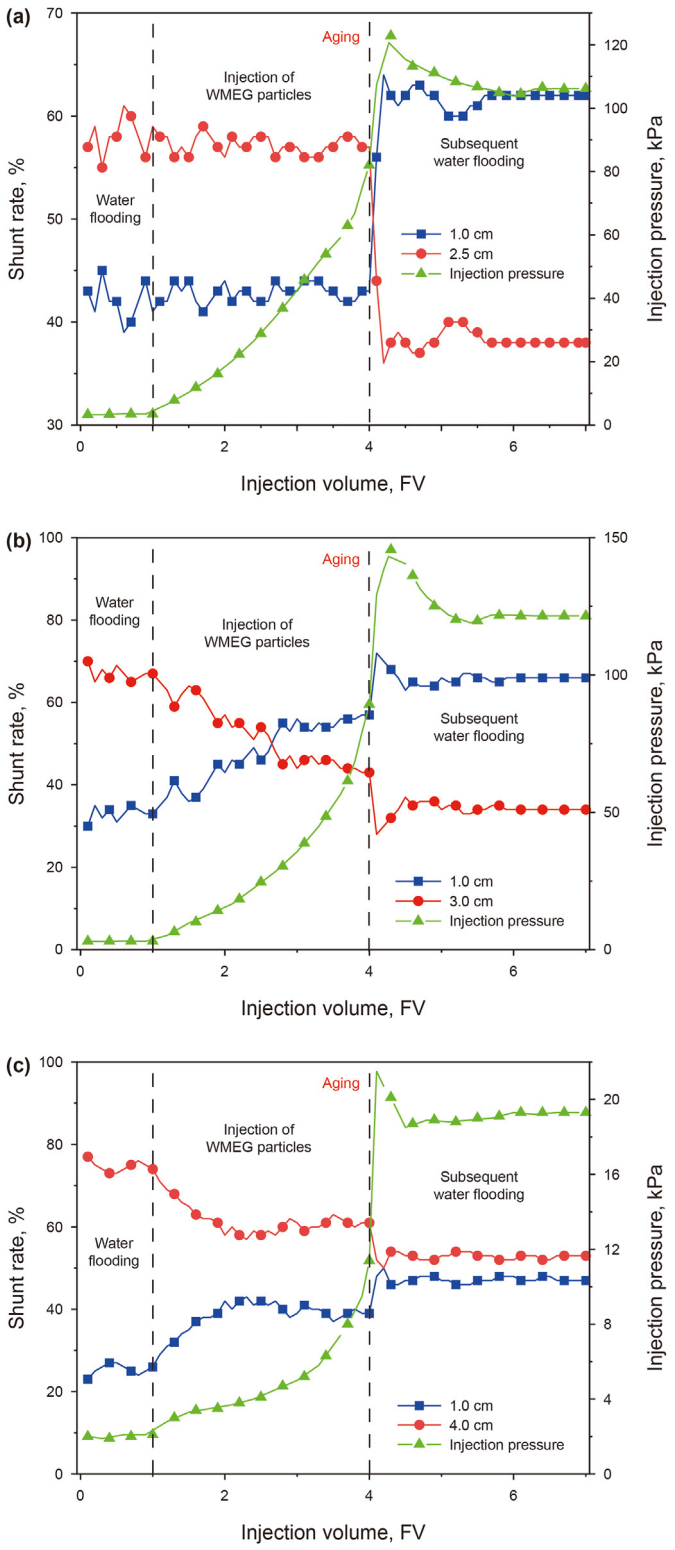

Fig. 13. Changes in the shunt rate and injection pressure of the WMEG particles with different fracture width ratios of 2.5 (**a**), 3.0 (**b**), and 4.0 (**c**).

The large fracture width cores usually have a larger diversion rate in the initial water flooding stage, which means that more water was produced from these cores. Therefore, the formation profile became more heterogeneous after long-term water flooding. Through injection of the WMEG particles, the injection pressure remarkably rises and the water generated by the low fracture width cores is gradually increased. When several FVs of water flooding continued, the injection pressure declined gradually to a constant value, and the water produced by the low fracture width cores further increased slightly. As a consequence, the profile control capacity of the WMEG particles reached 57.40%, 74.63%, and 68.68% at fracture ratios of 2.5, 3.0, and 4.0, respectively. From experiments (6), (7), and (8), the WMEG particles exhibits an excellent potential profile control capacity. This is explained by the special qualities of the WMEG particles. The WMEG particles can enter the big width fracture preferentially because of their potential for selection. For the special qualities of softness and self-lubrication, the WMEG particles are easily deformed and transported in the in-depth fracture. The expanded WMEG particles effectively plug in the fracture and force the injected water to redirect to the low width fracture. Therefore, the heterogeneous formation is improved and the fracture difference of cores is narrowed.

Table 2
Parameters of cores.

No.	Core parameters		
	Length, cm	Diameter, cm	Fracture width, mm
6	4.925	2.522.	2.5
7	5.014	2.513	3.0
8	4.958	2.486	4.0

3.8. Remaining oil distribution and EOR mechanism

An NMR displacement experimental device was utilized to study the distribution pattern and mechanism of residual oil. The analysis involved measuring T_2 spectra and MRI images at different displacement stages to understand the behavior of residual oil in the system. The experimental results are shown in Fig. 14.

Fig. 14(a) shows T_2 spectra before and after displacement, where the relaxation time T_2 reflects the specific surface area (SSA) of the pores and the signal amplitude reflects the oil saturation of the core. The color code in the MRI images represents the oil saturation in the core. The spatial dimension of the signal is proportional to the oil volume of the core, so the area difference between T_2 spectra determines oil recovery (Li J.M. et al., 2022). Due to the absence of oil in the matrix of the carbonate fractured reservoir, the signal within the range of $T_2 < 10$ ms (small pores) is 0. The signal mainly is distributed in the range of 10–1000 ms, indicating that the oil mainly comes from fractures, which also shows the reservoir function of fractures (Lang et al., 2009). When heavy water or the WMEG particles with heavy water flooding, the oil rich in hydrogen signal is gradually replaced from the core. The response in T_2 spectra and MRI images show that the signal amplitude decreases and the brightness of the MRI image decreases.

Fig. 14(b) shows that the brightness of the middle fracture decreases significantly after water flooding, indicating that the oil is displaced by heavy water. However, the oil in the upper and lower fractures is less developed. The injected water will preferentially enter the middle fracture under flooding pressure. Oil flows to the outlet, resulting in the signal decline of the middle fracture. After the injection of the WMEG particles, the middle fracture is plugged, which increases the resistance of water flooding to the middle fracture, so that a large amount of water enters the other fractures to replace oil. After aging, the volume of WMEG particles increases, which further enhances the flow resistance of the middle fracture. Subsequent water flooding results in significant displacement of oil within the three fractures, indicating the remarkable enhanced oil recovery capacity of the WMEG particles.

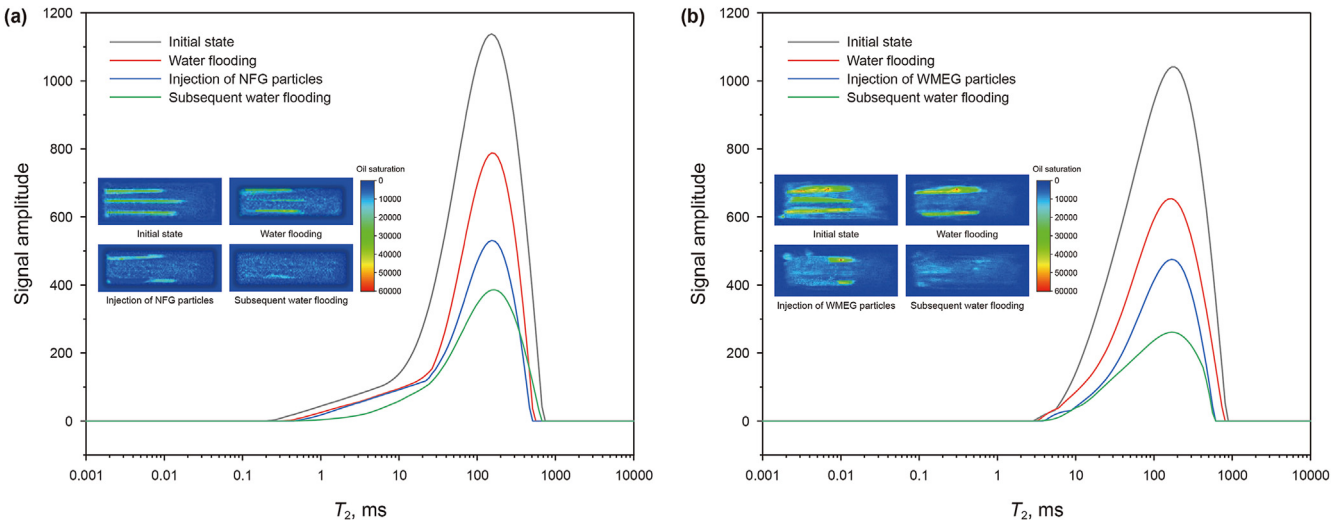

Fig. 14. T_2 spectra and MRI images at different flooding stages. (**a**) Injection of NFG particles; (**b**) Injection of WMEG particle system.

Table 3
Recovery proportion at each flooding stage of the NFG and WMEG particles.

Flooding system	Oil recovery, %			
	Water flooding	Injection of graphite particle system	Subsequent water flooding	Total
WMEG particles	41.5	21.0	13.3	75.8
NFG particles	41.9	18.2	8.6	68.7

To further analyze the capacity of the WMEG particles to enhance oil recovery. The recovery result of each flooding stage is shown in Table 3. The WMEG particle system demonstrates a 7.1% higher total recovery compared to the NFG particle system, providing conclusive evidence of the superior enhanced oil recovery capacity of the WMEG particles with expansive ability. The WMEG particles can be used as a temperature-tolerant and salt-tolerant profile control agent in carbonated reservoirs.

3.9. Profile control and EOR mechanism of the WMEG particles

To discuss the EOR mechanism of the WMEG particles, the profile control patterns of the WMEG particles was analyzed in this section. As shown in the SEM graphs, the typical characteristics of the fractures are shown in Fig. 15. After injecting water for a long time, these fractures with low flow resistance connect to form water predominant pathways. It is easy to form an invalid circulation of water injection when the injection water flows through these channels. Therefore, the oil recovery is difficult to improve under this situation. After the injection of the WMEG particles, these particles can directly pass and deform and pass the fractures in the formation. First, when the WMEG particles are injected into the fracture, it can stack in the fracture to plug the whole channel. Therefore, the flow resistance increases when the WMEG particle solution is injected. In addition, after entering the formation for a certain period, WMEG particles can also effectively plug fractures by thermal expansion. The flake structure of the expanded WMEG particles is further opened, and the volume is increased several times, which can directly plug some smaller fractures (Fig. 15(d)–(f)). Subsequently, the expanded WMEG particles greatly increase the water flow resistance and improve the injection profile of formation. Therefore, the increase in swept volume of the subsequent water flooding leads to the improvement of oil recovery.

Fig. 16 shows a schematic diagram of the WMEG particles plugging the channels to improve injection profile of formation. Long-term water injection creates the formation water channels in reservoirs (Fig. 16(a)). A significant amount of the subsequent injected water flows out of the wellbore through water channels, resulting in a waste of resources (Fig. 16(b)). At this time, a significant amount of residual oil remains in other fractures. To enhance the injection profile, the WMEG particle system is injected into the formation. WMEG particles will enter the water channels preferentially when they are inserted into the formation. Based on the softness and lubrication of WMEG particles, they can enter the part of water channels (Fig. 16(c)). The aging of the formation temperature causes the WMEG particles to gradually expand, leading to an increase in volume. Therefore the plugging effect of WMEG particles is further enhanced, resulting in subsequent water flooding into the unaffected zone, driving out the remaining oil and improving oil recovery (Fig. 16(d)).

4. Conclusions

In this work, WMEG particles were developed as a novel profile control agent and exhibited great potential for EOR treatment in carbonate reservoirs.

(1) The critical expansion temperature of the WMEG particles is 130 °C. High temperature promotes the expansion speed and expansion ratio of the WMEG particles, while salinity has almost no effect on the expansion performance. The volume of WMEG particles in solution and porous media can expand 3–8 times during aging under reservoir conditions. Compared with other in-depth profile control agents, WMEG particles can adapt to the high temperature and high salinity of deep reservoirs, and the higher the temperature, the better the plugging effect.

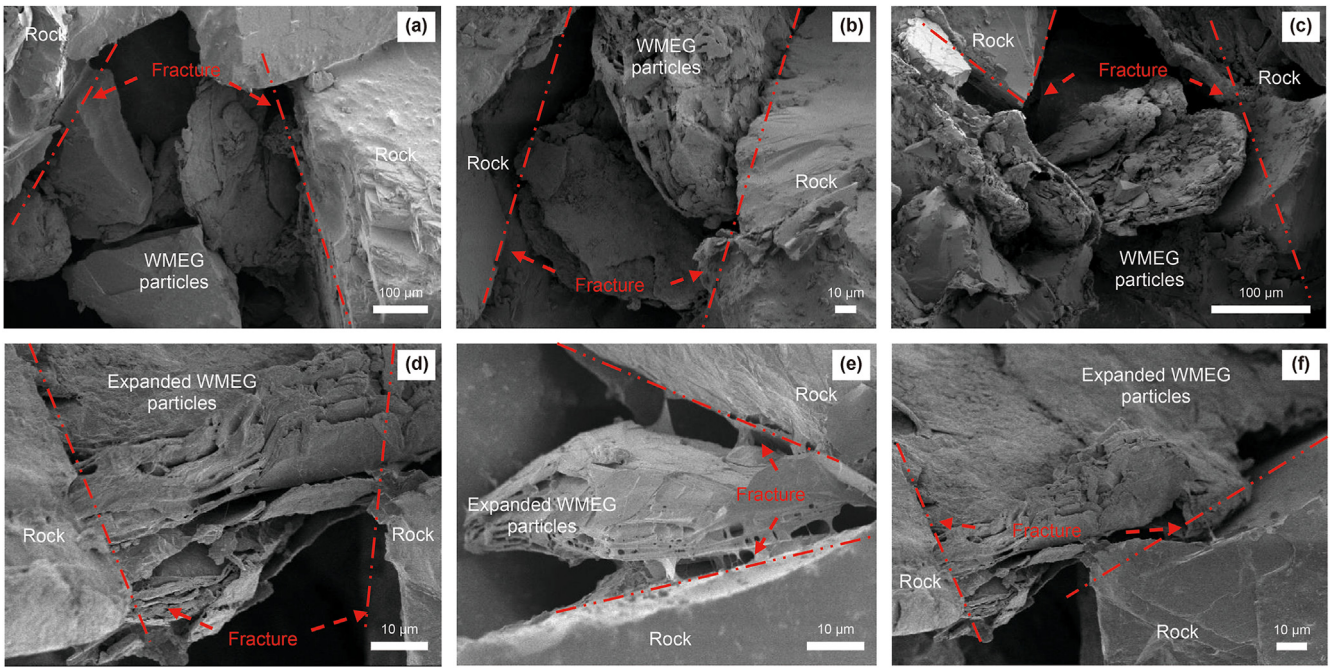

Fig. 15. Pattern of controlling water channels with the WMEG particles. (**a**)–(**c**) Plugging patterns of WMEG particles before aging; (**d**)–(**f**) Plugging patterns of the WMEG particles after aging.

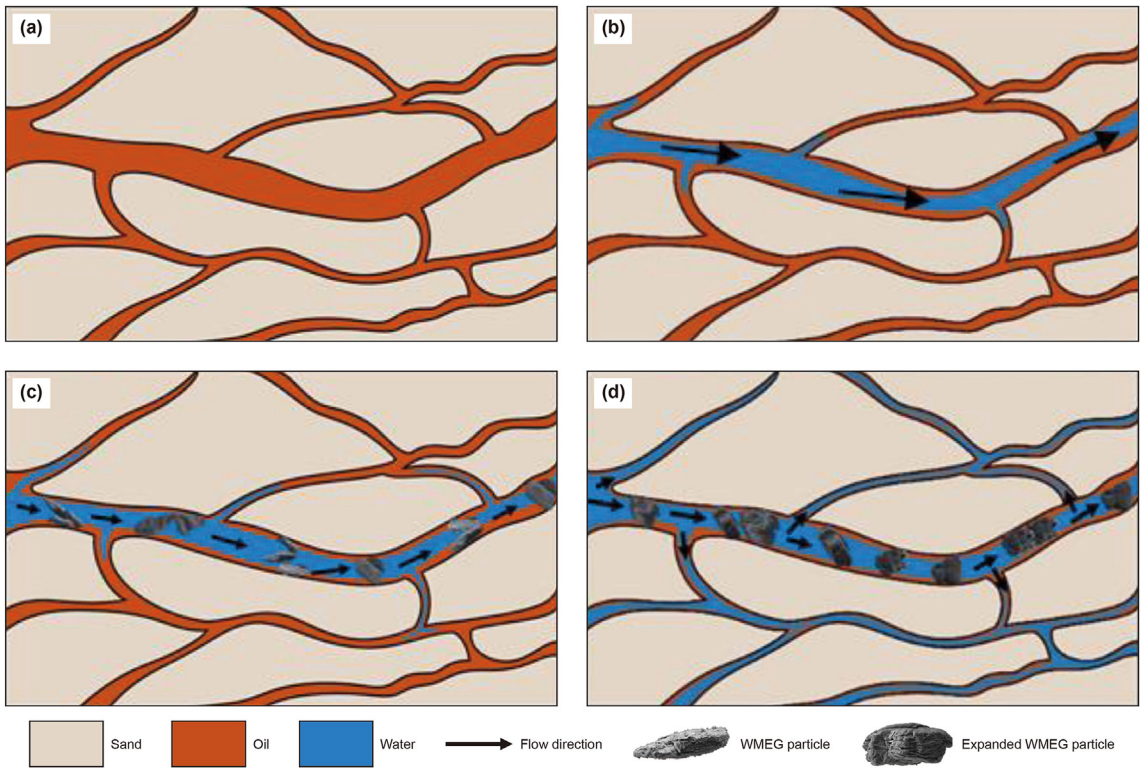

Fig. 16. Schematic diagram of water channel control of the WMEG particles. (**a**) Initial state; (**b**) Water flooding; (**c**) Injection of WMEG particle system; (**d**) Subsequent water flooding after aging.

(2) WMEG particles have the potential to immediately plug or bridge the fractures, thus enhancing reservoir homogeneity and efficiently plugging high-permeability water flow channels. Compared with conventional NFG particles, the expansion characteristic of WMEG particles strengthens their profile control capacity in reservoirs. Therefore, the follow-up water is forced to un-swept zones, and the swept volume was enlarged; thus, the residual oil is driven out.

(3) As low-cost inorganic particles, WMEG particles have a wide application prospect in in-depth profile control in deep reservoirs.

CRediT authorship contribution statement

Bo-Zhao Xu: Writing – review & editing, Writing – original draft, Validation, Supervision, Resources, Data curation, Conceptualization. **Dong-Fang Lv:** Supervision. **Dai-Yu Zhou:** Supervision, Resources. **Ning Sun:** Writing – review & editing, Supervision. **Si-Yu Lu:** Supervision. **Cai-Li Dai:** Validation, Resources. **Guang Zhao:** Writing – review & editing, Validation, Supervision, Funding acquisition. **Ming-Ming Shi:** Writing – review & editing, Validation, Resources.

Declaration of competing interest

The authors declare that they have no known competing financial interests or personal relationships that could have appeared to influence the work reported in this paper.

Acknowledgments

This work is financially supported by the National Natural Science Foundation of China (No. 52074335), China University of Petroleum (East China) Independent Innovation Research Program: Oilfield Chemistry and Enhanced Oil Recovery (27RA2302015), Innovation Fund Project for Graduate Student of China University of Petroleum (East China) and the Fundamental Research Funds for the Central Universities (No. 24CX04003A).

References

Almohsin, A., Hung, J., Alabdrabalnabi, M., Sherief, M., 2021. A nano method for a big challenge: nanosilica-based sealing system for water shutoff. In: SPE Middle East Oil & Gas Show and Conference. https://doi.org/10.2118/204840-MS.

Alshehri, A.J., Wang, J., Kwak, H.T., AlSofi, A.M., Gao, J., 2019. A study of gel-based conformance control within fractured carbonate cores using low-field nuclear-magnetic-resonance techniques. SPE Reservoir Eval. Eng. 22 (3), 1063–1074. https://doi.org/10.2118/187397-PA.

Asl, F.O., Zargar, G., Manshad, A.K., Iglauer, S., Keshavarz, A., 2022. Experimental investigation and simulation for hybrid of nanocomposite and surfactant as EOR process in carbonate oil reservoirs. Fuel 319, 123591. https://doi.org/10.1016/j.fuel.2022.123591.

Bai, Y.-R., Zhang, Q.-T., Sun, J.-S., Jiang, G.-C., Lv, K.-H., 2022. Double network self-healing hydrogel based on hydrophobic association and ionic bond for formation plugging. Petrol. Sci. 19 (5), 2150–2164. https://doi.org/10.1016/j.petsci.2022.07.006.

Boeije, C., Rossen, W., 2017. SAG foam flooding in carbonate rocks. Journal of Petroleum Science and Science 741, 843–853. https://doi.org/10.1016/j.petrol.2018.08.017.

Bruno, R. Cancela, Palermo, L.C.M., Oliveira, P.F.d., Mansur, C.R.E., 2022. Rheological study of polymeric fluids based on HPAM and fillers for application in EOR. Fuel 330, 125647. https://doi.org/10.1016/j.fuel.2022.125647.

Dai, C., Fang, J., Jiao, B., Long, He, He, X., 2018. Development of the research on EOR for carbonate fractured-vuggy reservoirs in China. J. China Univer. Petrol. (Ed. Nat. Sci.) 42 (6), 67–78. https://doi.org/10.3969/j.issn.1673-5005.2018.06.008 (in Chinese).

Ding, X., Dai, C., Sun, Y., Zhu, M., Liu, Y., Chang, Y., Zhao, G., You, Q., Shaikh, A., 2021. Conformance control study by micrometer sized dispersed particle gel in three-dimensional tight oil fracture network. J. Petrol. Sci. Eng. 197, 108112. https://doi.org/10.1016/j.petrol.2020.108112.

Du, L., Xiao, Y.Y., Jiang, Z.C., Zeng, H.B., Li, H.Z., 2023. Towards in-depth profile control using dispersed particle gels (DPGs). Fuel 354. https://doi.org/10.1016/j.fuel.2023.129419.

Ge, J., Wu, H., Song, L., Zhang, T., Li, L., Guo, H., 2021. Preparation and evaluation of soft preformed particle gels for conformance control in carbonate reservoir. J. Petrol. Sci. Eng. 205, 108774. https://doi.org/10.1016/j.petrol.2021.108774.

Gong, X., Zhu, M., Wu, G., Wang, C., Zhang, Q., 2016. Performance evaluation and application of ultrafine powder plugging agent. Oilfield Chem 33 (2), 248–253. https://doi.org/10.19346/j.cnki.1000-4092.2016.06.013 (in Chinese).

Gussenov, I., Nuraje, N., Kudaibergenov, S., 2019. Bulk gels for permeability reduction in fractured and matrix reservoirs. Energy Rep. 5, 733–746. https://doi.org/10.1016/j.egyr.2019.06.012.

Jin, F.-y., Jiang, T.-t., Varfolomeev, M.A., Yuan, C., Zhao, H.-y., He, L., Jiao, B.-l., Du, D.-j., Xie, Q., 2021. Novel preformed gel particles with controllable density and its implications for EOR in fractured-vuggy carbonated reservoirs. J. Petrol. Sci. Eng. 205, 108903. https://doi.org/10.1016/j.petrol.2021.108903.

Karadkar, P., Almohsin, A., Bataweel, M., Huang, J., 2023. In-situ pore plugging using nanosilica-based fluid system for gas shutoff to maximize oil production. SPE Prod. Oper. 8 (1), 104–112. https://doi.org/10.2118/197578-PA, 3.

Lang, D., Shang, G., Lv, C., Shaoping, D., Sun, A., Shang, X., 2009. Experiment and application of NMR in carbonate reservoir analysis an example from Tahe oilfield. Oil Gas Geol 30 (3), 363–369. https://doi.org/10.11743/ogg20090317 (in Chinese).

Li, J.M., Zhao, G., Sun, N., Liang, L.H., Yang, N., Dai, C.L., 2022. Construction and evaluation of a graphite oxide Nanoparticle-Reinforced polymer flooding system for enhanced oil recovery. J. Mol. Liq. 367. https://doi.org/10.1016/j.molliq.2022.120546.

Li, Q., Yu, X., Wang, L., Qu, S., Wu, W., Ji, R., Luo, Y., Yang, H., 2022. Nano-silica hybrid polyacrylamide/polyethylenimine gel for enhanced oil recovery at harsh conditions. Colloids Surf. A Physicochem. Eng. Asp. 633, 127898. https://doi.org/10.1016/j.colsurfa.2021.127898.

Liu, D., Shi, X., Zhong, X., Zhao, H., Pei, C., Zhu, T., Zhang, F., Shao, M., Huo, G., 2017. Properties and plugging behaviors of smectite-superfine cement dispersion using as water shutoff in heavy oil reservoir. Appl. Clay Sci. 147, 160–167. https://doi.org/10.1016/j.clay.2017.07.030.

Liu, P., Jiang, L., Tang, B., Ren, K., Huang, M., Geng, C., 2022. Residual oil distribution pattern in a fault-solution carbonate reservoir and countermeasures to improve oil development effectiveness. Geofluids 2022. https://doi.org/10.1155/2022/2147200.

Liu, Z., Bode, V., Hadayati, P., Onay, H., Sudhölter, E.J.R., 2020. Understanding the stability mechanism of silica nanoparticles: the effect of cations and EOR chemicals. Fuel 280, 118650. https://doi.org/10.1016/j.fuel.2020.118650.

Lu, J., Wan, X., Azzolina, N.A., Bosshart, N.W., Zhao, J., Yu, Y., Yu, X., Smith, S.A., Sorensen, J.A., Gorecki, C.D., 2022. Optimizing conformance control for gas injection EOR in unconventional reservoirs. Fuel 324, 124523. https://doi.org/10.1016/j.fuel.2022.124523.

Luo, M., Jia, X., Si, X., Luo, S., Zhan, Y., 2021. A novel polymer encapsulated silica nanoparticles for water control in development of fossil hydrogen energy—tight carbonate oil reservoir by acid fracturing. Int. J. Hydrogen Energy 46 (61), 31191–31201. https://doi.org/10.1016/j.ijhydene.2021.07.022.

Mehrabianfar, P., Malmir, P., Soulgani, B.S., Hashemi, A., 2020. Study on the optimization of the performance of preformed particle gel (PPG) on the isolation of high permeable zone. J. Petrol. Sci. Eng. 195, 107530. https://doi.org/10.1016/j.petrol.2020.107530.

Salem Ragab, A.M., Hannora, A.E., 2015. A Comparative investigation of nano particle effects for improved oil recovery–experimental work. In: SPE Kuwait Oil and Gas Show and Conference. https://doi.org/10.2118/175395-MS.

Song, C., Lu, X., Hou, J., Ma, C., Qu, M., Tan, T., Guo, C., 2023. Preparation and performance evaluation of reinforced foam system with high temperature resistance and high salt tolerance in fracture-cavity reservoirs in Tahe Oilfield. Petrol. Geol. Recov. Efficien. 30 (5), 76–83. https://doi.org/10.13673/j.cnki.cn37-1359/te.202209053 (in Chinese).

Sun, N., Yao, X., Liu, J., Li, J., Yang, N., Zhao, G., Dai, C., 2023. Breakup and coalescence mechanism of high-stability bubbles reinforced by dispersed particle gel particles in the pore-throat micromodel. Geoenergy Sci. Eng. 223, 211513. https://doi.org/10.1016/j.geoen.2023.211513.

Wang, H.W., Zhao, Z.L., Gao, Z.W., Ding, Y.A., Yang, D.Y., 2022. Experimental and mechanistic characterizations of oil-based cement slurry flow behavior through fractures in a carbonate reservoir. J. Energy Resour. Tech.-Transact. Asme 144 (12). https://doi.org/10.1115/1.4054704.

Wu, Q.-H., Ge, J.-J., Ding, L., Zhang, G.-C., 2023. Unlocking the potentials of gel conformance for water shutoff in fractured reservoirs: favorable attributes of the double network gel for enhancing oil recovery. Petrol. Sci. 20 (2), 1005–1017. https://doi.org/10.1016/j.petsci.2022.10.018.

Wu, W.-P., Hou, J.-R., Qu, M., Yang, Y.-L., Zhang, W., Wu, W.-M., Wen, Y.-C., Liang, T., Xiao, L.-X., 2022. A novel polymer gel with high-temperature and high-salinity resistance for conformance control in carbonate reservoirs. Petrol. Sci. 19 (6), 3159–3170. https://doi.org/10.1016/j.petsci.2022.05.003.

Wu, W., Qin, F., Ouyang, D., He, L., 2015. Study on water plugging technology in fractured-cavity carbonate reservoirs, Tahe oilfield. Petrol. Geol. Recov. Efficien. 20 (6), 104–107 (in Chinese).

Xu, B.Z., Zhao, G., Gu, C.L., Dai, C.L., Zhao, W.X., Ma, T.T., 2023. Research and application progress of wet-phase modified expandable graphite as a steam plugging agent in heavy oil reservoirs. Energy & Fuels. 37 (2), 1081–1091. https://doi.org/10.1021/acs.energyfuels.2c03811.

Zhao, G., Dai, C.L., Gu, C.L., You, Q., Sun, Y.P., 2019. Expandable graphite particles as a novel in-depth steam channeling control agent in heavy oil reservoirs. Chem. Eng. J. 368, 668–677. https://doi.org/10.1016/j.cej.2019.03.028.

Zhu, D.-Y., Luo, R.-T., Liu, Y., Qin, J.-H., Zhao, Q., Zhang, H.-J., Wang, W.-S., Wang, Z.-Y., Zhu, M.-E., Wang, Y.-P., Li, P.-B., 2022. Development of re-crosslinkable dispersed particle gels for conformance improvement in extremely high-temperature reservoirs. Petrol. Sci. 19 (6), 2922–2931. https://doi.org/10.1016/j.petsci.2022.05.017.